Published as:
Gomez, F., Karam, G., Khawlie, M., McClusky, S., Vernant, P., Reilinger, R., Jaafar, R., Tabet, C., Khair, K., and Barazangi, M., 2007. Global Positioning System measurements of strain accumulation and slip transfer through the restraining bend along the Dead Sea fault system in Lebanon, *Geophysical Journal International,* 168, 1021-1028.

Global Positioning System measurements of strain accumulation and slip transfer through the restraining bend along the Dead Sea fault system in Lebanon

Francisco Gomez[1], Gebran Karam[2], Mohamad Khawlie[3], Simon McClusky[4], Philippe Vernant[4], Robert Reilinger[4], Rani Jaafar[1], Charles Tabet[5], Kamal Khair[6], Muawia Barazangi[7]

[1]Department of Geological Sciences, University of Missouri, Columbia, Missouri 65211
[2]Department of Civil Engineering, Lebanese American University, Jbail, Lebanon
[3]Lebanese National Center for Remote Sensing, Beirut, Lebanon
[4]Department of Earth, Atmospheric, and Planetary Sciences, Massachusetts Institute of Technology, Cambridge, Massachusetts 02139
[5]Lebanese National Council for Scientific Research, Beirut, Lebanon
[6]Hasbaya, Lebanon
[7]Institute for the Study of the Continents, Snee Hall, Cornell University, Ithaca, New York 14853

Abbreviated title: GPS Measurements in Lebanon

Corresponding Author: Francisco Gomez
Department of Geological Sciences
University of Missouri
Columbia, Missouri 65211
USA

phone: +1 573 882 9744
fax: +1 573 882 5458
e-mail: fgomez@missouri.edu

Total Number of Words (not including References): 2940

Summary

Approximately four years of campaign and continuous GPS measurements across the Dead Sea fault system in Lebanon provide direct measurements of interseismic strain accumulation along a 200-km-long restraining bend in this continental transform fault. Late Cenozoic transpression within this restraining bend has maintained more than 3,000 meters of topography in the Mount Lebanon and Anti-Lebanon ranges. The GPS velocity field indicates 4 – 6 mm/yr of relative plate motion is transferred through the restraining bend to the northern continuation of the Dead Sea fault system in northwestern Syria. Near-field GPS velocities are generally parallel to the major, left-lateral strike-slip faults, suggesting that much of the expected convergence across the restraining bend is likely accommodated by different structures beyond the aperture of the GPS network (e.g., offshore Lebanon and, possibly, the Palmyride fold belt in SW Syria). Hence, these geodetic results suggest a partitioning of crustal deformation involving strike-slip displacements in the interior of the restraining bend, and crustal shortening in the outer part of the restraining bend. Within the uncertainties, the GPS-based rates of fault slip compare well with Holocene-averaged estimates of slip along the two principle strike-slip faults: the Yammouneh and Serghaya faults. Of these two faults, more slip occurs on the Yammouneh fault, which constitutes the primary plate boundary structure between the Arabia and Sinai plates. Hence, the Yammouneh fault is the structural linkage that transfers slip to the northern part of the transform in northwestern Syria. From the perspective of the regional earthquake hazard, the Yammouneh fault is presently locked and accumulating interseismic strain.

Key Words: Crustal deformation, Dead Sea fault system, Global Positioning System (GPS), Fault motion, Neotectonics, Transform faults

Introduction

The central part of the Dead Sea fault system in Lebanon and southwestern Syria is a ~200 km long restraining bend that strikes 25 - 30 degrees from the main trend of the transform (Figure 1). Within the geodynamic framework of the eastern Mediterranean region, the left-lateral Dead Sea fault system (DSFS) is the continental transform boundary between the Arabian and Sinai plates (e.g., Freund *et al.* 1970; McKenzie 1972), accommodating the differential motion of those two plates as they converge and collide with Eurasia.

Although late Cenozoic strike-slip movements of the DSFS are well documented (e.g., Quennell 1958; Freund *et al.* 1970), some debate has persisted over the past decade concerning the present-day activity of the northern DSFS and whether or not plate motion is presently transmitted through the restraining bend (Girdler 1990; Butler *et al.* 1998). This debate was motivated, primarily, by the apparent lack of instrumentally recorded seismicity along the restraining bend and the northern portion of the transform in NW Syria. Specific questions concerning the DSFS include: Is strain presently accumulating within the restraining bend? If so, how is crustal deformation distributed? How do short-term (geodetic) estimates of fault slip compare with long-term (late Quaternary) estimates?

Whether or not the central DSFS is an active restraining bend also pertains to broader questions of how large restraining bends in major transcurrent fault systems develop. Faults within restraining bends typically have orientations that are not optimal with regard to the regional plate motions (i.e., the boundary forces). Yet restraining bends persist, often involving increased structural complexity compared with the rest of the fault system.

This “Lebanese” restraining bend compares in scale to other large restraining bends, such as the Big Bend along the San Andreas fault system in southern California. Late Cenozoic transpression within the Lebanese restraining bend has uplifted the Mount Lebanon and Anti Lebanon ranges to elevations in excess of 3,000 meters. Similar to the San Andreas fault system within the Big Bend, the single trace of the southern DSFS splays into several structures within the Lebanese restraining bend (Walley 1988) (Figure 2): The Yammouneh, Serghaya, Rachaya, Roum, and Akkar faults. Of those, the Yammouneh fault appears to be the only through-going structure that connects the southern and northern parts of the DSFS. The Serghaya fault, the other major NNE-SSW strike-slip fault, seems to terminate in the northern Anti Lebanon range (Gomez *et al.* 2003; Gomez *et al.* 2006). Two faults striking oblique to the transform, the Roum

fault in the south and the Akkar fault in the north, appear to serve as the structural linkages between the strike-slip faults of the restraining bend and horizontal shortening of the Mount Lebanon range (e.g., Gomez *et al.* 2006; Nemer & Meghraoui 2006).

Geodetic estimates of present-day plate motion along the DSFS are relatively slow at 4 – 6 mm/yr. (e.g., Wdowinski *et al.* 2004; Mahmoud *et al.* 2005). This is consistent with longer return periods (500 – 1000 years) for strike-slip earthquakes within the Lebanese restraining bend (e.g., Gomez *et al.* 2003; Meghraoui *et al.* 2003; Daeron *et al.* 2005). Despite a general seismic quiescence at the present time, historical records document numerous large earthquakes within the restraining bend, most notably in 551 AD, 1202 AD, 1759 AD, and 1837 AD (e.g., Sbeinati *et al.* 2005). Hence, understanding the active crustal deformation, particularly in terms of strain accumulation and the earthquake cycle, is critical to improving the estimates of the regional earthquake hazard.

Recent paleoseismic and neotectonic studies within the Lebanese restraining bend have helped constrain the late Pleistocene / Holocene kinematics of several major faults: Purely strike-slip displacement is documented along the Yammouneh fault (4 – 6 mm/yr) and Serghaya fault (1 – 1.5 mm/yr) (Gomez *et al.* 2003; Daeron *et al.* 2004; Gomez *et al.* 2007). Along the Roum fault, a strike-slip rate of 1 mm/yr in the south grades into increased dip slip toward the northern end of the fault (Nemer & Meghraoui 2006).

This study reports the initial GPS velocity field for the Lebanese restraining bend along the Dead Sea fault system. The results provide permit kinematic modeling of the restraining bend and quantify the accumulation of interseismic strain along the Yammouneh fault.

GPS Measurements and Data Processing

The regional GPS network used in this study includes one local continuous GPS station (LAUG) with 14 survey monuments (Figure 2). Monumentation at the 14 survey sites consisted of 10 cm steel pins cemented into bedrock. Sites were distributed about Lebanon in order to facilitate 2-dimensional analysis of the resulting velocities. The campaign sites were repeatedly measured during 5 survey campaigns between spring 2002 and fall 2005. In each campaign, sites were observed for a minimum of 24 hours using Trimble 5700 receivers with Zephyr

geodetic antennae atop fixed-height antenna masts in order to reduce uncertainty owing to antenna setup.

GPS data were processed in a two-step procedure using the GAMIT/GLOBK software (Herring *et al.* 1997; Dong *et al.* 1998; King & Bock 1998). In the first step, loosely constrained estimates of station coordinates, orbital and Earth orientation parameters, and atmospheric zenith delays were determined from raw GPS observables using GAMIT. Data from the Lebanon GPS network were analyzed along with raw GPS data from other continuously operating GPS stations in the region. Subsequently, a global Kalman filter (GLOBK) was applied to the combined, loosely constrained solutions and their associated covariances in order to estimate a consistent set of station coordinates and velocities. As part of this second step, a 6 parameter transformation was estimated by minimizing the horizontal velocities of 49 globally distributed IGS stations with respect to the IGS00 realization of the ITRF 2000 no-net-rotation reference (NNR) frame. A "random walk" noise of 1 mm / $\sqrt{}$yr was also assumed in the final velocity estimation.

After stabilizing the reference frame, the site velocities were resolved to an Arabian-fixed reference frame, which facilitates assessing the local deformation. Velocities (in NNR and Arabia-fixed reference frames) for the sites around the Lebanese restraining bend are provided in Table 1.

Results and Modeling

Figure 2 depicts the resulting velocity field around the Lebanese restraining bend. Uncertainties for the resulting velocities are typically less than 1 mm/yr (1 sigma). In the Arabia-fixed reference frame shown in Figure 2, the sites along the Lebanese coast demonstrate SSW motion of the Sinai plate relative to Arabia. South of the restraining bend, the velocities rotate to a more southward direction, maintaining their fault-parallel orientation.

Within the central part of the restraining bend, velocity variations along a WNW-ESE profile (i.e., perpendicular to the NNE-SSW strike of the Yammouneh and Serghaya faults, see Figure 2) permit an initial kinematic assessment. The profiles in Figure 3 decompose the velocities into motions parallel and perpendicular to the Yammouneh and Serghaya faults. These profiles deliberately exclude GPS survey sites at the extremities of the restraining bend and those which might be complicated by the obliquely striking Roum fault. The velocities parallel to the

transform (Figure 3a) show a progressive increase in southward velocity from east to west – a pattern that is generally consistent with basic models of elastic strain accumulation (e.g., Savage & Burford 1973). In addition to this strike-slip deformation, the fault-normal components of displacement (Figure 3b) suggest up to 2 mm/yr of motion (i.e., shortening) between sites in the Anti Lebanon (TFEL and ARSL) and the continuous station along the Lebanese coast (LAUG).

An initial, quantitative assessment of the geodetic slip rate is based on a 1-dimensional elastic dislocation model of a locked fault. Following Savage & Burford (1973), this profile model assumes an infinitely long strike-slip fault and expresses the station velocity, b, as a function of the long-term slip rate (V), fault locking depth (D), and distance from the fault (x):

$$b = (V/\pi) \tan^{-1} (x/D). \quad (1)$$

Owing to the size of the uncertainties relative to the velocities, present observations, warrant only a single fault model (i.e., the Yammouneh fault). Despite the simplifications and assumptions, this analytical model permits assessing a range of values of fault slip rates and locking depths consistent with the GPS data using a grid search. The 1-sigma contour shown in Figure 3c is based on a Mote Carlo simulation to assess the noise level in the data (e.g., Sandvol & Hearn 1994). As demonstrated in Figures 3a and 3c, the entire range of geological slip estimates (3.5 – 6.5 mm/yr) can be modeled to fit nearly all of the velocities, with locking depths of 8 to 25 km. As shown in Figure 3c, the peak of the probability distribution corresponds with a slip rate of 4.4 mm/yr and a locking depth of 13 km.

A more appropriate elastic model and robust estimate of the fault slip rate involves 2-dimensional blocks bounded by faults of finite lengths, rather than a 1-dimensional profile. This modeling follows the methodology of Meade & Hager (2005), and considers the spatial variations in the velocity field due to fault geometry, and the effect of block rotations that are not accounted for in 1-D models and can both significantly impact deduced slip rates. In this approach, an optimal fit between plate motion, fault slip, and GPS velocities is determined using a linearized least squares inverse method. In our 2-dimensional modeling, we assume a fault locking depth of 15 km because present uncertainties preclude solving for this additional parameter. Furthermore, the anticipated ~1.5 mm/yr of slip along the Serghaya fault is less than the 2-sigma uncertainties for the present results. Hence, the present block model is simplified to a single fault bend.

The residual fit to the optimal model is shown in Figure 4, along with derived components of strike-slip and fault-normal movement. Within the restraining bend, a left-lateral slip rate of 3.8 ± 0.3 mm/yr (formal uncertainty reflecting only data fit and not uncertainties in fault parameters) is inferred, along with 1.6 ± 0.4 mm/yr of convergence across the fault. South of the restraining bend, a slip rate of 4.0 ± 0.3 mm/yr is accompanied with a small component of extension (0.8 ± 0.3 mm/yr), whereas north of the restraining bend, 4.2 ± 0.3 mm/yr of strike-slip is accompanied by an insignificant component (0.2 ± 0.5 mm/yr) of convergence across the DSFS. As previously noted, late Pleistocene / Holocene slip rates along the Yammouneh fault suggest a slip rate of 3 – 6 mm/yr, and the block model is consistent with the lower end of this range.

Discussion

Our GPS velocities conclusively demonstrate the present-day accumulation of strain along left-lateral faults in central and northern Lebanon. Furthermore, the velocity field yields insight into the kinematics of slip transfer through this restraining bend. Specifically, the velocity field demonstrates: (1) the predominance of strike-slip faulting inside the restraining bend, and (2) less shortening than is expected from plate motions. These observations are consistent with regional strain partitioning that involves strike-slip displacements in the core of the restraining bend, and crustal shortening in the outer part of the restraining bend.

The velocity vectors in Figure 2 bend parallel to the major strike-slip faults through the restraining bend. This is well demonstrated by the northward change in the orientations from BSHM (south of the restraining bend) to JIYE and LAUG (within the restraining bend). With the near-field constraints, the elastic block model suggests rates of strike-slip faulting that are similar inside and outside the restraining bend – i.e., the rates of strike-slip do not decrease significantly as might be expected from a simple, geometric decomposition of plate motion into slip perpendicular and parallel to the restraining bend (e.g., Gomez *et al.* 2003).

Our elastic block model suggests about 1.6 mm/yr of convergence across the restraining bend – nearly half of the convergence compared with the regional block model of Reilinger *et al.* (2006). The model of Reilinger *et al.* (2006) constrained the motion along the Dead Sea fault system solely with continuous GPS stations (primarily in the far-field), whereas our model

includes additional survey sites in the near-field of the restraining bend. We suggest this difference may, in part, reflect the fact that the GPS stations in Lebanon do not measure the full convergence, and this may bias the block model.

In an analogous study of the Big Bend along the San Andreas fault system, Lisowski *et al.* (1991) concluded that the convergent component across a restraining bend seems to be accommodated across a zone with a width comparable to the length of the bend. Applying this to the Lebanese restraining bend suggests that sites along the Lebanese coast would not be expected to demonstrate the total convergent component of motion – some of convergence may be accommodated offshore, as suggested by recent studies (e.g., Briais *et al.* 2004)). Additionally, seismicity in the Palmyride fold belt suggests that some of the shortening associated with the Lebanese restraining bend may be accommodated by internal deformation of the northern Arabian plate (e.g., Chaimov *et al.* 1990). Hence, owing to the low rate of convergence across the Lebanese restraining bend and the width of the zone over which the elastic strain accumulates, we believe that measurement of the full convergence may be below the detection threshold of our current GPS observations.

Although the residuals for the block model are smaller than the uncertainties, an apparently systematic westward residual motion may reflect the need for a more complicated model involving reverse faults to accommodate WNW-ESE directed crustal shortening. Alternatively, a dip on the Yammouneh fault could be added to accommodate plate motion with oblique slip. However, landforms offset by the Yammouneh fault demonstrate only strike-slip displacements (e.g., Daeron *et al.* 2004; Gomez *et al.* 2007) – therefore, shortening perpendicular to the sub-vertically dipping Yammouneh fault is likely accommodated by a different structures.

These GPS measurements, as with recent paleoseismic studies, unambiguously refute suggestions that the plate boundary is located offshore to the west (e.g., Butler *et al.* 1998). The DSFS within the restraining bend is active despite the significant obliquity of plate motion relative to the restraining bend. Hence, changes in relative motion between the Arabian and Sinai plates (Garfunkel 1981; Butler *et al.* 1998) did not cause a change in this plate boundary as suggested by Butler *et al*. The persistence of the restraining bend implies that the DSFS is sufficiently weaker than the surrounding continental crust such that it is mechanically preferable to reactivate the transform, rather than develop new faults.

Conclusions

The GPS results presented herein provide direct geodetic measurement of present-day fault slip transferring through the Lebanese restraining bend. The GPS velocities maintain their fault parallel orientation along the restraining bend indicating that regional compression required by Sinai-Arabia relative plate motion is accommodated by structures other than the main through-going Yammouneh strike-slip fault. Fault slip rates deduced from simple elastic models constrained by the GPS results are consistent with the total 4 – 6 mm/yr of relative plate motion between the Arabia and Sinai plates, and generally consistent with the lower range of geological estimates of slip rates along the Yammouneh fault. The displacement field suggests that the Yammouneh fault accommodates most of the expected strike-slip motion – hence, the DSFS (and specifically the Yammouneh fault) represents the main Sinai-Arabia plate boundary.

The GPS measurements also yield initial constraints on near-field deformation around the northern Dead Sea fault system. The near-field velocities suggest that the Yammouneh fault is presently accumulating strain. Hence, the apparent lack of present-day seismicity is likely a reflection of the slow rates of strain accumulation about a locked fault system. These results reinforce concerns about earthquake potential of the Yammouneh fault, which has a historical record of producing large earthquakes (M ~ 7.5) (Sbeinati *et al.* 2005).

Acknowledgements

This research has been supported in part by NSF grants EAR-0439021 to Missouri, NSF EAR-0439807 to MIT, and EAR-0106238 to Cornell University. Tom Herring and Bob King provided guidance with data processing. We acknowledge the support of the Lebanese American University administration with maintenance of the continuous GPS station. Field assistance was provided by Chadi Abdallah, Chris Boujaoudi, Ihab Jomaa, Jihad Shuman, and Amin Shaban. This manuscript also benefited from helpful discussions with Eric Sandvol and Tony Nemer.

References Cited

Briais, A., Singh, S. C., Tapponnier, P., Elias, A., Sursock, A., Jomaa, R., Carton, H., Daeron, M., King, G. & Jacques, E., 2004. Neogene and active shortening offshore the reactivated Levant margin in Lebanon: results of the SHALIMAR cruise, *2004 Fall AGU Meeting*, San Francisco.

Butler, R. W. H., Spencer, S. & Griffiths, H. M., 1998. The structural response to evolving plate kinematics during transpression: evolution of the Lebanese restraining bend of the Dead Sea Transform. *In:* Holdsworth, R. E., Strahan, R. A. & Dewey, J. F. (eds) *Continental Transpressional and Transtensional Tectonics*. Geological Society (London). Special Publications, 135, 81-106.

Chaimov, T. A., Barazangi, M., Al-Saad, D., Sawaf, T. & Gebran, A., 1990. Crustal shortening in the Palmyride fold belt, Syria, and implications for movement along the Dead Sea fault system. *Tectonics*, 9, 1369-1386.

Daeron, M., Benedetti, L., Tapponnier, P., Sursock, A. & Finkel, R. C., 2004. Constraints on the post ~25-ka slip rate of the Yammouneh fault (Lebanon) using in situ cosmogenic 36Cl dating of offset limestone-clast fans. *Earth Planet. Sci. Lett.*, 227, 105-119.

Daeron, M., Klinger, Y., Tapponnier, P., Elias, A., Jacques, E. & Sursock, A., 2005. Sources of the large A.D. 1202 and 1759 Near East earthquakes. *Geology*, 33, 529-532.

Dong, D., Herring, T. A. & King, R. W., 1998. Estimating regional deformation from a combination of space and terrestrial geodetic data. *J. Geod.*, 71, 200-211.

Freund, R., Garfunkel, Z., Zak, I., Goldberg, M., Weissbrod, T. & Derin, B., 1970. The shear along the Dead Sea rift. *Philosophical Transactions of the Royal Society of London, Series A*, 267, 107-130.

Garfunkel, Z., 1981. Internal structure of the Dead Sea leaky transform (rift) in relation to plate kinematics. *Tectonophysics*, 80, 81-108.

Girdler, R. W., 1990. The Dead Sea transform fault ystem. *Tectonophysics*, 180, 1-13.

Gomez, F., Meghraoui, M., Darkal, A. N., Hiajzi, F., Mouty, M., Suleiman, Y., Sbeinati, R., Darawcheh, R., Al-Ghazzi, R. & Barazangi, M., 2003. Holocene faulting and earthquake recurrence along the Serghaya branch of the Dead Sea fault system in Syria and Lebanon. *Geophys. J. Int.*, 153, 658-674.

Gomez, F., Khawlie, M., Tabet, C., Darkal, A. N., Khair, K. & Barazangi, M., 2006. Neotectonics of the northern Dead Sea fault system in Lebanon and Syria based on SAR imagery and high resolution DEM data. *Earth Planet. Sci. Lett.*, 241, 913-931.

Gomez, F., Nemer, T., Tabet, C., Khawlie, M., Meghraoui, M. & Barazangi, M., 2007. Strain partitioning of active transpression within the Lebanese Restraining Bend of the Dead Sea fault (Lebanon and SW Syria). *In:* Cunningham, D. & Mann, P. (eds) *Tectonics of Strike-Slip Restraining & Releasing Bends in Continental & Oceanic Settings*. Geological Society of London Special Publication, in press.

Herring, T. A., King, R. W. & McClusky, S. C., 1997. Geodetic constraints on interseismic, coseismic, and postseismic deformation in southern California. *Annual Report to SCEC*,

King, R. W. & Bock, Y., 1998. *Documentation of MIT GPS analysis software: GAMIT*. Massachusetts Institute of Techology, Cambridge, MA,

Lisowski, M., Savage, J. C. & Prescott, W. H., 1991. The velocitiy field along the San Andreas fault in central and southern California. *J. geophys. Res.*, 96, 8369-8389.

Mahmoud, S., Reilinger, R., McClusky, S., Vernant, P. & Tealeb, A., 2005. GPS evidence for northward motion of the Sinai block: Implications for E. Mediterranean tectonics. *Earth Planet. Sci. Lett.*, 238, 217-227.

McKenzie, D., 1972. Active tectonics of the Mediterranean region. *Geophys. J. RAS*, 30, 109-185.

Meade, B. J. & Hager, B., 2005. Block models of crustal motion in southern California constrained by GPS measurements. *J. geophys. Res.*, 110, doi: 10.1029/2004JB003209.

Meghraoui, M., Gomez, F., Sbeinati, R., Van der Woerd, J., Mouty, M., Darkal, A. N., Radwan, Y., Layyous, I., Al Najjar, H., Darawcheh, R., Hijazi, F., Al-Ghazzi, R. & Barazangi, M., 2003. Evidence for 830 years of seismic quiescence from palaeoseismology, archaeosesimology, and historical seismicity along hte Dead Sea fault in Syria. *Earth Planet. Sci. Lett.*, 210, 35-52.

Nemer, T. & Meghraoui, M., 2006. Evidence of coseismic ruptures along the Roum fault (Lebanon): A possible source for the AD 1837 earthquake. *Journal of Structural Geology*, in press.

Quennell, A. M., 1958. The structural and geomorphic evolution of the dead sea rift. *Quarterly Journal of the Geological Society (London)*, 64, 1-24.

Reilinger, R., McClusky, S., Vernant, P., Lawrence, S., Ergintav, S., Cakmak, R., Kadirov, F., Guliev, I., Stepanyan, R., Mahmoud, S., Sakr, K., ArRajehi, A., Paradissis, D., Al-Aydrus, A., Evren, E., Dmitrotsa, A., Filikov, S. V., Gomez, F., Al-Ghazzi, R. & Karam, G., 2006. GPS Constraints on Continental Deformation in the Africa-Arabia-Eurasia Continental Collision Zone and Implications for the Dynamics of Plate Interactions. *J. geophys. Res.*, 111, doi:10.1029/2005JB004051.

Sandvol, E. & Hearn, T., 1994. Bootstrapping shear-wave splitting errors. *Bulleting of the Seismological Society of America*, 84, 1971-1977.

Savage, J. C. & Burford, R. O., 1973. Geodetic determination of relative plate motion in central California. *J. geophys. Res.*, 78, 832-845.

Sbeinati, M. R., Darawcheh, R. & Mouty, M., 2005. Catalog of historical earthquakes in and around Syria. *Ann. Geofis.*, 48, 347-435.

Walley, C. D., 1988. A braided strike-slip model for the northern continuation of the Dead Sea Fault and its implications for Levantine tectonics. *Tectonophysics*, 145, 63-72.

Wdowinski, S., Bock, Y., Baer, G., Prawirodirdjo, L., Bechor, N., Naaman, S., Knafo, R., Forrai, Y. & Melzer, Y., 2004. GPS measurements of curent crustal movements along the Dead Sea Fault. *J. geophys. Res.*, 109, 54035-418.

Table 1. Velocities of GPS sites shown in Figure 2

			ITRF 2000		Arabia-fixed			
Site	Long	Lat	Vel E	Vel N	Vel E	Vel N	σE	σN
ARSL	36.467	34.174	22.21	5.33	-1.66	0.22	0.94	0.91
HRML	36.369	34.412	20.37	3.65	-3.33	-1.42	0.91	0.85
UDMC	36.285	33.510	24.69	3.47	0.37	-1.57	0.91	0.91
TFEL	36.235	33.860	19.71	5.16	-4.37	0.13	0.88	0.88
BRKA	36.143	34.194	22.03	3.66	-1.81	-1.34	0.80	0.77
HABT	36.084	34.461	21.22	4.18	-2.43	-0.79	0.74	0.74
ANJR	35.922	33.740	22.03	3.63	-2.12	-1.29	0.76	0.77
ADAS	35.899	34.466	22.23	2.92	-1.40	-1.99	0.78	0.78
HZRT	35.880	33.859	21.43	4.52	-2.63	-0.38	0.82	0.78
FRYA	35.829	34.015	21.97	2.70	-1.98	-2.19	0.78	0.79
ELRO	35.771	33.182	23.11	3.60	-1.42	-1.26	0.61	0.60
HAYT	35.762	34.089	19.44	0.71	-4.46	-4.15	0.78	0.79
MCHK	35.761	33.516	20.92	2.76	-3.38	-2.10	0.78	0.77
LAUG	35.674	34.115	21.60	1.06	-2.27	-3.77	0.86	0.87
JZIN	35.579	33.545	21.70	1.40	-2.57	-3.40	0.77	0.76
JIYE	35.401	33.641	20.90	3.03	-3.29	-1.70	0.78	0.79
RBDA	35.162	33.149	21.43	0.55	-3.09	-4.10	0.87	0.89
KABR	35.145	33.023	22.70	1.45	-1.91	-3.19	0.61	0.60
BSHM	35.023	32.779	24.56	0.63	-0.21	-3.97	0.69	0.68

Figure Captions

Figure 1. Regional tectonic map of the Dead Sea fault system. Also shown are the relative plate motions (Arabia vs. Sinai) predicted by Reilinger et al. (2006). Abbreviations: EAF = East Anatolian fault, NAF = North Anatolian fault.

Figure 2. Map showing general structure of the Lebanese restraining bend. GPS velocities for the network used in this study are also shown in an Arabia-fixed reference frame (2-sigma uncertainties). Abbreviations for some key tectonic features: RF = Roum fault, RaF = Rachaya fault, AF = Akkar fault, & PFB = Palmyride fold belt. Box denotes the swath encompassed by the profiles in Figure 3.

Figure 3. Plots showing GPS velocities (a) parallel and (b) perpendicular to the Yammouneh fault across the central part of the Lebanese restraining bend (positive N and E, respectively). The fault parallel velocities also include predicted velocities for different elastic dislocation models (i.e., combinations of locking depth and slip rate). The locations of the Yammouneh (solid) and Serghaya (dashed) faults are shown, although the model in 3a only includes the former. See Figure 2 for location. (c) A plot depicting the 1-sigma confidence limits on slip rate and locking depth. Confidence limits are based on a grid search approach and a Monte Carlo simulation to estimate the noise level in the data. The peak of the probability distribution corresponds with a slip rate of 4.4 mm/yr and a locking depth of 14 km.

Figure 4. Map depicting elastic block model of a bend along a single fault trace. Strike-slip and fault-normal components of slip are shown for each segment. Heavy red lines denote fault segments under extension, and heavy blue lines denote fault segments with orthogonal shortening. Residuals of the velocities (mm/yr) to the best model and 2-sigma uncertainties are also shown.

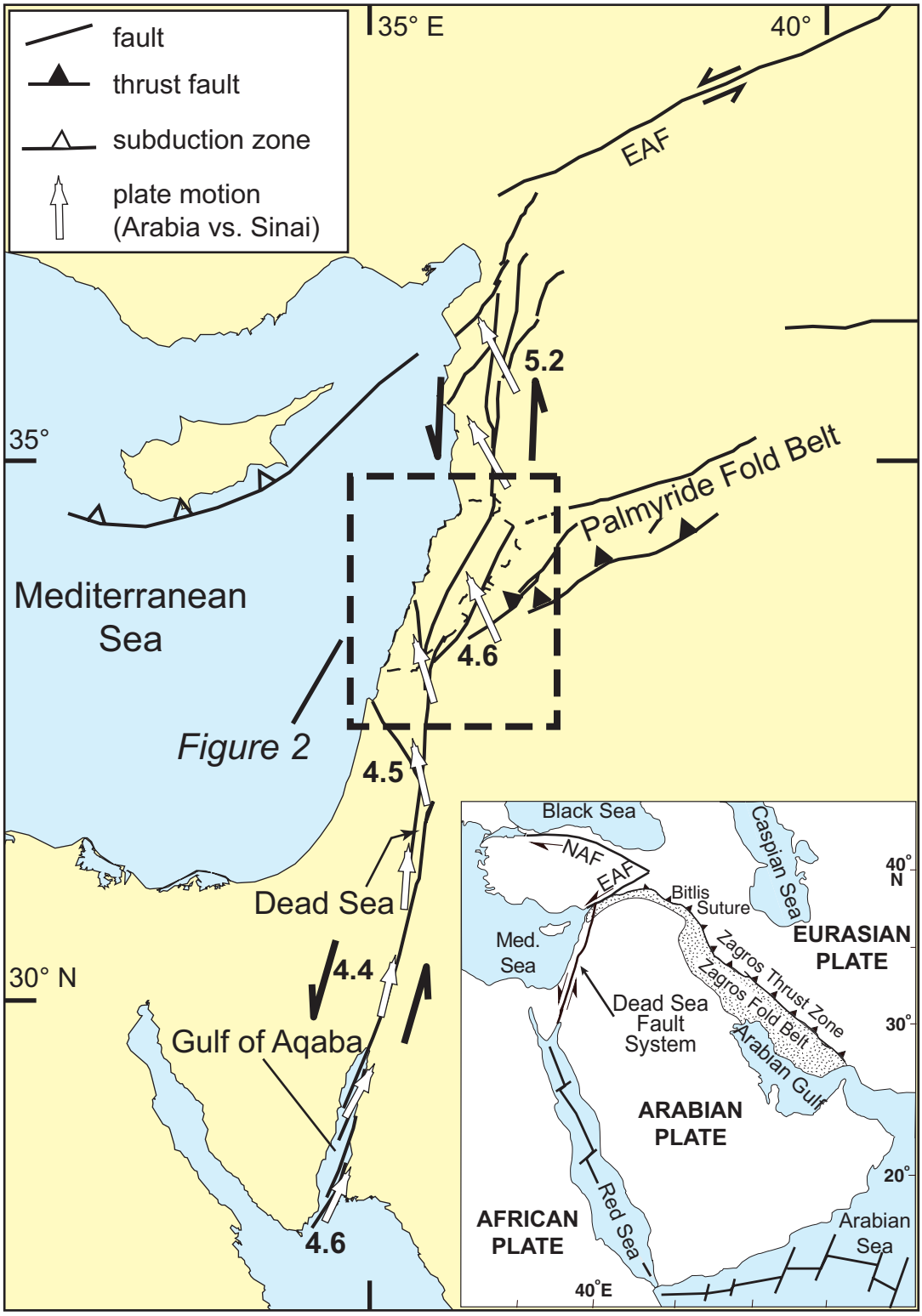

Figure 1
Gomez et al.

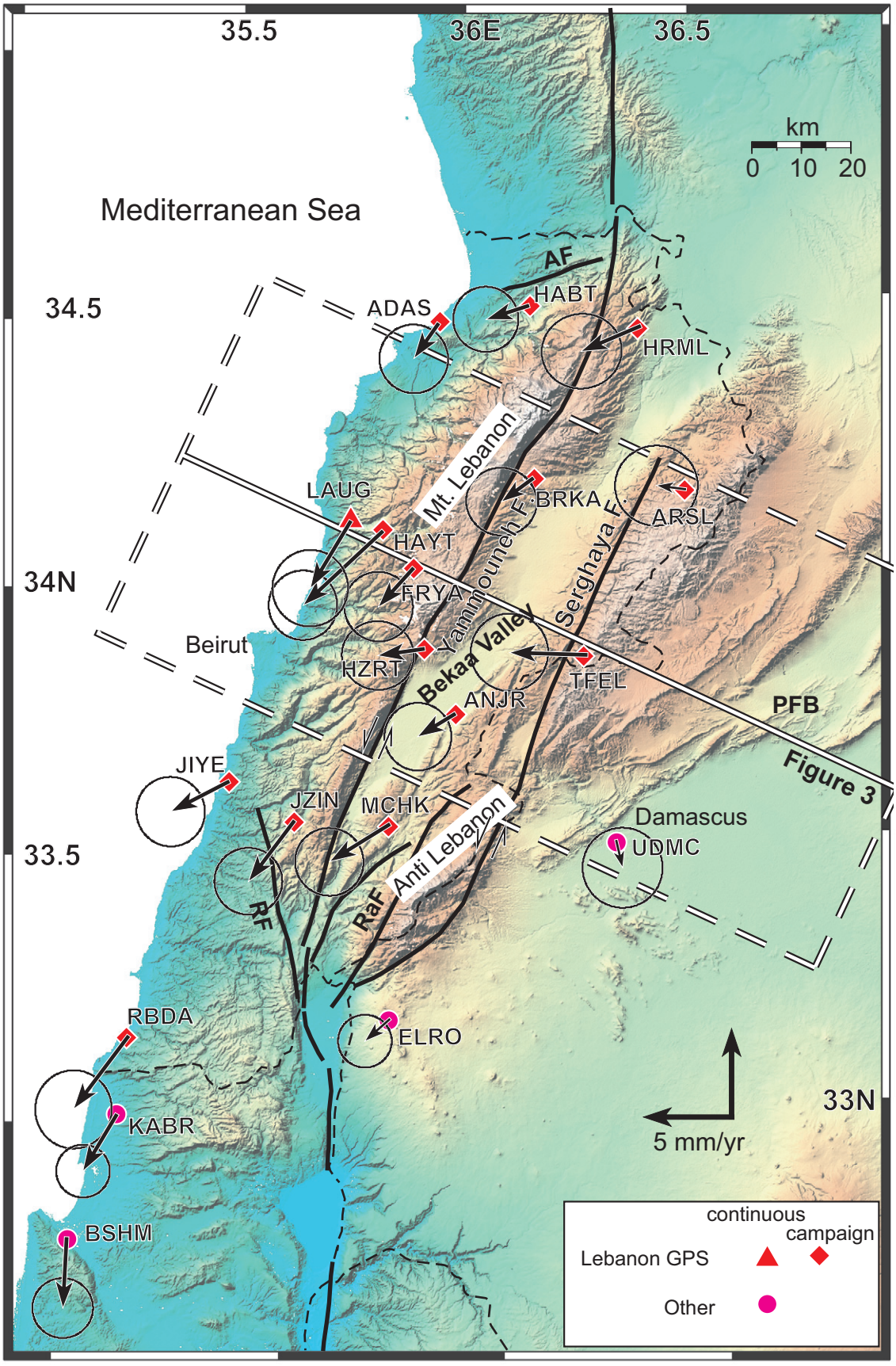

Figure 2
Gomez et al.

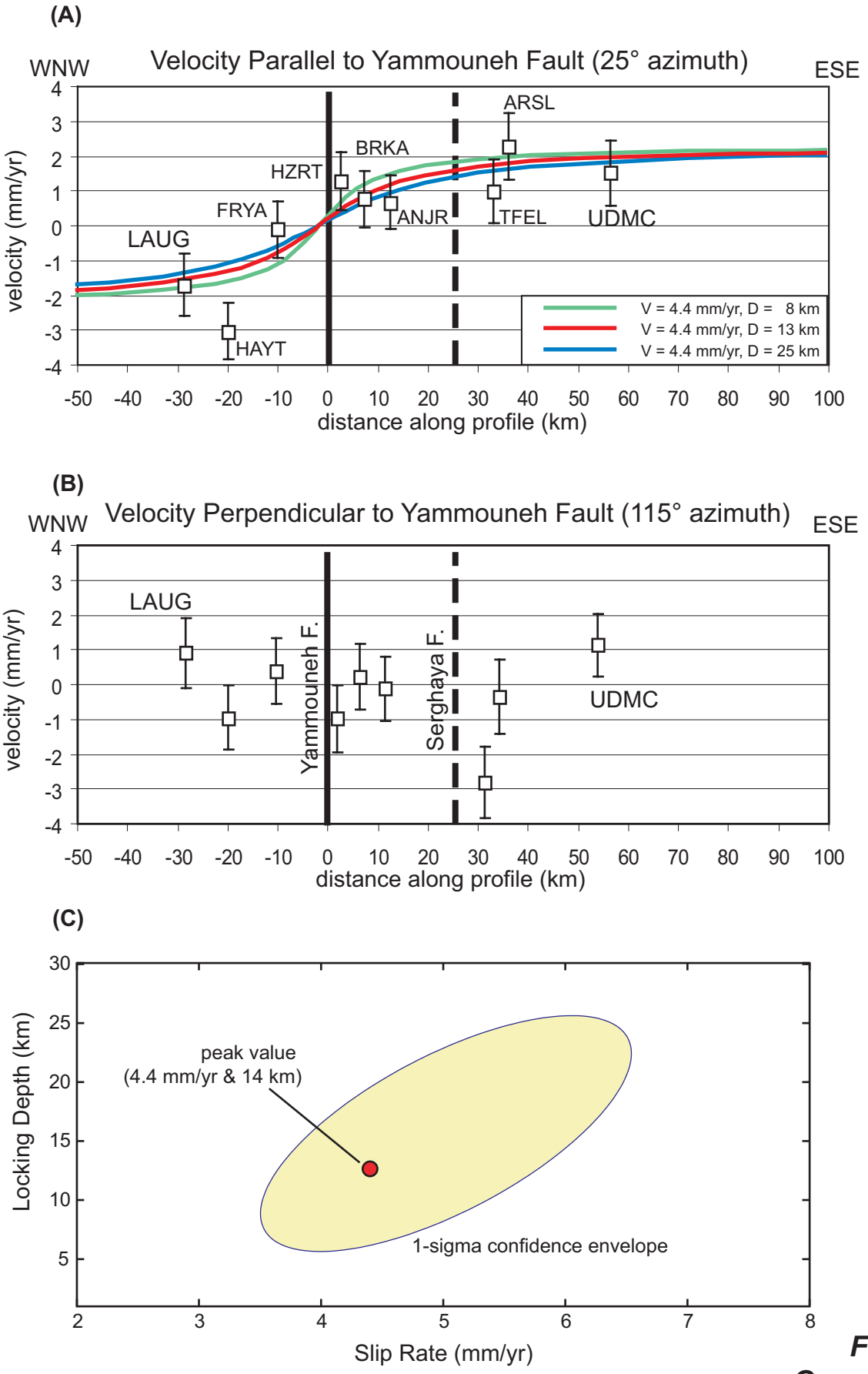

Figure 3
Gomez et al.

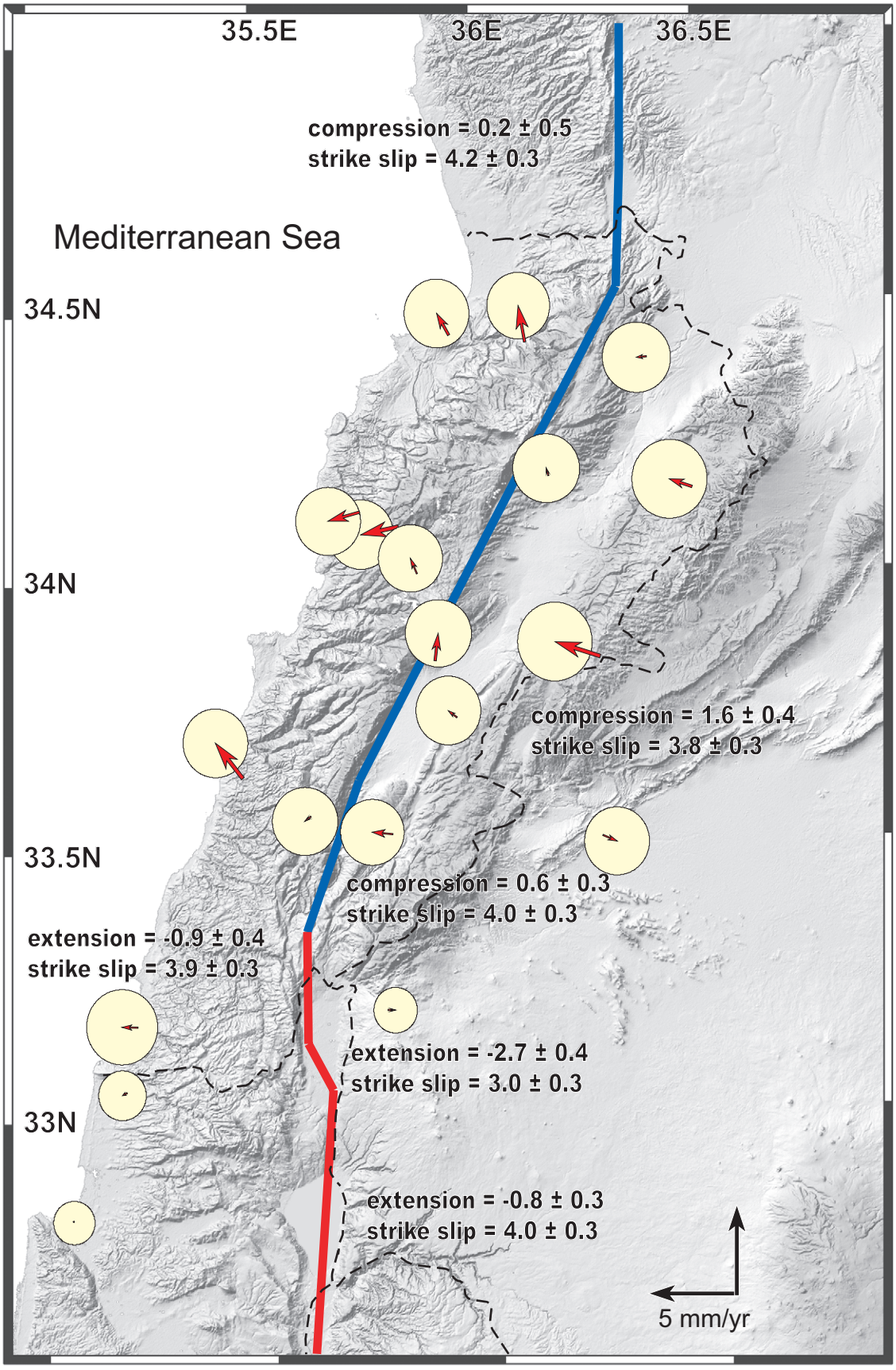

Figure 4
Gomez et al.